

Three-dimension hierarchical heterostructure of CdWO₄ microrods decorated with Bi₂WO₆ nanoplates for high-selectivity photocatalytic benzene hydroxylation to phenol



Peng Chen^a, Lang Chen^{a,*}, Yu Zeng^a, Feng Ding^a, Xu Jiang^a, Na Liu^a, Chak-Tong Au^b, Shuang-Feng Yin^{a,*}

^a State Key Laboratory of Chemo/Biosensing and Chemometrics, Provincial Hunan Key Laboratory for Cost-effective Utilization of Fossil Fuel Aimed at Reducing Carbon-dioxide Emissions, College of Chemistry and Chemical Engineering, Hunan University, Changsha 410082, Hunan, China

^b College of Chemistry and Chemical Engineering, Hunan Institute of Engineering, Xiangtan 411104, Hunan, China

ARTICLE INFO

Keywords:

Hierarchical heterostructure
Photocatalysis
Selective hydroxylation
Phenol
Bi₂WO₆/CdWO₄

ABSTRACT

For the first time Bi₂WO₆/CdWO₄ (BCW) hierarchical heterostructure of CdWO₄ microrods decorated with uniform Bi₂WO₆ nanoplates was prepared. Using BCW as photocatalyst and O₂ as oxidant, we achieved satisfactory catalytic activity (benzene conversion 7.3% and selectivity of phenol > 99%) in the hydroxylation of benzene to phenol at room temperature. It was found that the unique hierarchical heterostructure is beneficial for the absorption of visible light and the separation of photoinduced charge carriers. Moreover, we confirm the pivotal role of hydroxyl radicals and propose a plausible mechanism for the hydroxylation reaction.

1. Introduction

Given the high demand of phenol in chemical industries [1], the selective oxidation of benzene to phenol under mild conditions is a big challenge [2]. Recently, the selective hydroxylation of benzene to phenol through photocatalytic processes has attracted much interest from the viewpoint of environment friendliness [3,4]. Homogeneous and heterogeneous photocatalysts were reported for such an end [5–7], albeit with shortcomings. In a homogeneous system it is difficult to separate the catalyst from the product, while in a heterogeneous system the leaching of active species is likely [8]. Of the heterogeneous photocatalysts, those based on g-C₃N₄ and TiO₂ require the use of noble metals and/or ultraviolet radiation [9–11]. What is more, among the most reported heterogeneous catalytic systems, H₂O₂ was used as oxidant. It is hence timely to develop photocatalysts that are superior in terms of activity for the selective hydroxylation of benzene using greener oxidant such as O₂.

With suitable band composition, unique layered structure, relatively high photocatalytic activity and good stability, Bi₂WO₆ has been widely researched for the selective oxidation of glycerol, reduction of CO₂, selective oxidation of saturated alpha-carbon C–H bonds and the degradation of organic dyes [12–17]. However, because of the rapid combination of photogenerated electrons and holes and poor light absorption ability, the performances of Bi₂WO₆ photocatalysts are not

satisfactory [18]. For effective utilization of solar energy, hierarchical nanostructures with specific morphology have been extensively studied for the tailoring of physical and chemical properties [19]. Generally, having interconnected pores of different lengths and with large surface area and accessible space, low-density hierarchical materials of variable chemical compositions are favorable for light harvesting, electron and ion transport, as well as mass loading and diffusion [20]. Therefore, considerable effort has been put in to synthesize hierarchical photocatalysts so as to achieve high activities. In addition, the coupling of Bi₂WO₆ with CdWO₄ to form heterojunctions can restrain the combination of photogenerated electrons and holes [21].

In the present work, for the first time Bi₂WO₆/CdWO₄ (BCW) with hierarchical heterostructure was synthesized for photocatalytic applications. In the hierarchical heterostructure, CdWO₄ microrods are decorated with Bi₂WO₆ nanoplates that are uniform in size and shape. We examined the photocatalysis of BCW in the selective hydroxylation of benzene to phenol using O₂ as oxidant, and investigated the effect of Bi₂WO₆/CdWO₄ molar ratio. Besides, we investigated the pivotal role of hydroxyl radicals (·OH) photogenerated from Bi₂WO₆/CdWO₄ and propose a plausible mechanism for the reaction.

* Corresponding authors.

E-mail addresses: huagong042cl@163.com (L. Chen), sf_yin@hnu.edu.cn, yinsf73@163.com (S.-F. Yin).

2. Experimental section

2.1. Preparation of CdWO₄ microrods

Cd(NO₃)₂·4H₂O (1.234 g) and ethylenediamine (0.24 g) were dissolved in deionized water (20 mL). After vigorous stirring of the resulted solution for 10 min, 20 mL of an aqueous solution containing 1.316 g of Na₂WO₄·2H₂O was added dropwise under continuous stirring. The pH value was adjusted to 7 using aqueous nitric acid solution. After stirring for another 20 min, the mixture was transferred to a Teflon-lined stainless steel autoclave of 100 mL, and filled up to 80% of filling capacity with deionized water. The autoclave was sealed and maintained at 160 °C for 20 h and then cooled down to room temperature. The product was collected by centrifugation and washed three times with deionized water. Finally it was dried at 80 °C for 4 h.

2.2. Synthesis of BCW

Bi(NO₃)₃·5H₂O and Na₂WO₄·2H₂O in molar ratio of 2:1 were mixed in 30 mL of ethylene glycol (EG) and the solution was transferred to a Teflon-lined autoclave. Then 1 mmol of CdWO₄ rods and a desired amount of Bi₂WO₆ precursor were added to the autoclave. The autoclave was sealed and heated to 160 °C for 24 h. After the solvothermal treatment, the as-synthesized sample was washed with deionized water and ethanol for thorough removal of ionic residual before being dried in an oven at 80 °C for 4 h. The as-obtained samples with nominal Bi:Cd molar ratios of 1:10, 2:10, 3:10, 4:10, 5:10 and 7:10 are labelled hereinafter as BCW-1, BCW-2, BCW-3, BCW-4, BCW-5 and BCW-7, respectively. For comparison, Bi₂WO₆ nanoparticles without CdWO₄ rods were prepared according to the solvothermal method.

2.3. Photocatalytic activity measurements

The oxidation reactions were carried out in a three-necked round-bottom flask fixed with a reflux condenser. In a typical experiment, 0.5 mmol of benzene, 100 μL of water and 3 mL of acetonitrile together with 50 mg of catalyst were added into the flask, and dioxygen (3 mL/min) was introduced to the bottom of the reaction mixture. Prior to irradiation, the mixture was magnetically stirred in the dark for 30 min to establish adsorption-desorption equilibrium. After a designated period of irradiation (a 300 W Xe lamp (PLS-SXE 300 C, Perfectlight) with a 400 nm cut off filter), the oxygen flow was stopped and the catalyst was recovered by means of centrifugation. The products were identified using a Shimadzu GCMS-QP2010 ultra mass spectrometer and quantified over a Shimadzu GC 2010 Plus chromatograph equipped with a FID and a WAX capillary column (30 m × 0.25 mm × 0.25 μm). The conversion of benzene and yield of phenol were estimated by gas chromatography (GC 2010 Plus). The internal standard method was

employed with decane as internal standard.

2.4. Catalyst characterizations

Powder X-ray diffraction (XRD) pattern of samples was collected on a Bruker D8 Advance X-ray diffractometer with mono-chromatized Cu-Kα radiation ($\lambda = 0.154\text{ }06\text{ nm}$). The morphology and microscopic structure were observed over a field emission scanning electron microscope (FE-SEM, Hitachi S-4800) as well as a high-resolution transmission electron microscope (HR-TEM, JEM-2100F). X-ray photoelectron spectroscopy (XPS) was used to determine the Bi 4f, Cd 3d, W 4f and O 1 s binding energies (BEs) of surface bismuth, cadmium, tungsten and oxygen species, using Mg-Kα ($h\nu = 1253.6\text{ eV}$) as excitation source (XPS, SSX-100, Mg-Kα). The UV-vis diffuse reflectance spectra (UV-vis DRS) were recorded over a Cary-100 spectrophotometer, using BaSO₄ as background reference. The specific surface area of the as-prepared samples was studied by N₂ adsorption and desorption method at low temperature using a NOVA 1000e instrument (Quantachrome Instruments, USA), adopting the Brunauer-Emmet-Teller formula for calculation. The FTIR spectra were recorded with an IR Affinity-1 FTIR spectrometer (Shimadzu, Japan). Briefly, about 5.0 mg of each sample was added to 100 mg of KBr for pulverizing. Then, the FTIR spectra were recorded between 4000 and 400 cm⁻¹ at 4 cm⁻¹ intervals.

2.5. Photo-electrochemical measurements

The photocurrent was measured on a CHI660B electrochemical workstation using a standard three-electrode system. A platinum wire electrode, standard calomel electrode in saturated KCl and the as-prepared catalysts were used as counter electrode, reference electrode and working electrode, respectively. The working electrode was immersed in a sodium sulfate electrolyte solution (0.2 M) and illuminated with visible light. To prepare the working electrode, 50 mg of photocatalyst was dispersed in 5 mL of deionized water under ultra-sonic treatment for 30 min. The suspension was then dip-coated for several times onto a 2 × 2 cm² fluorine-doped tin oxide glass electrode, and for each time the conductive glass was dried at 60 °C for 30 min before the next dip.

3. Results and discussion

The scanning electron microscopy (SEM) images of CdWO₄ and BCW-4 are shown in Fig. 1. CdWO₄ is in the form of microrods with smooth surface, having diameters range from 700 to 900 nm and length from 3–8 μm (Fig. 1a). In Fig. 1b, one can see that Bi₂WO₆ nanoplates grow vertically, covering the entire surface of the CdWO₄ microrods. The Bi₂WO₆ nanoplates in the form of two-dimensional layers are packed next to each other in an orderly manner. Such a hierarchical heterostructure is generally favorable for photocatalytic action because

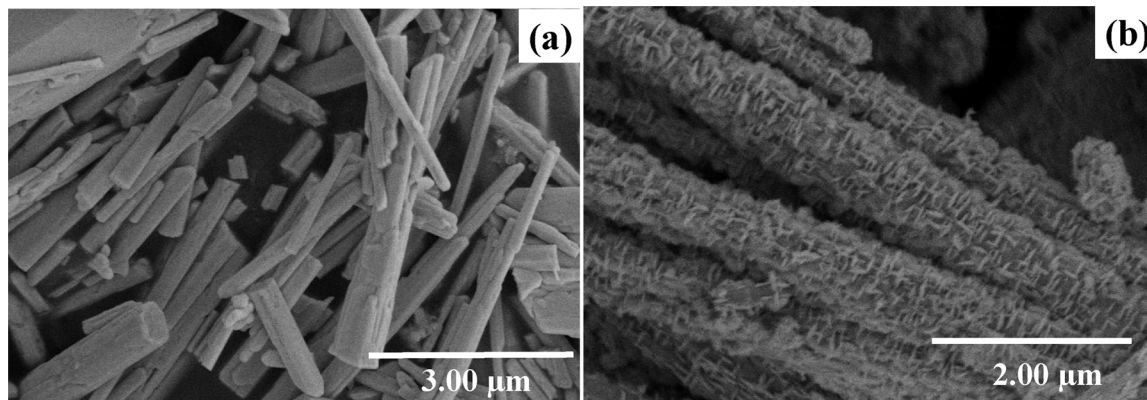


Fig. 1. SEM images of (a) CdWO₄ and (b) BCW-4.

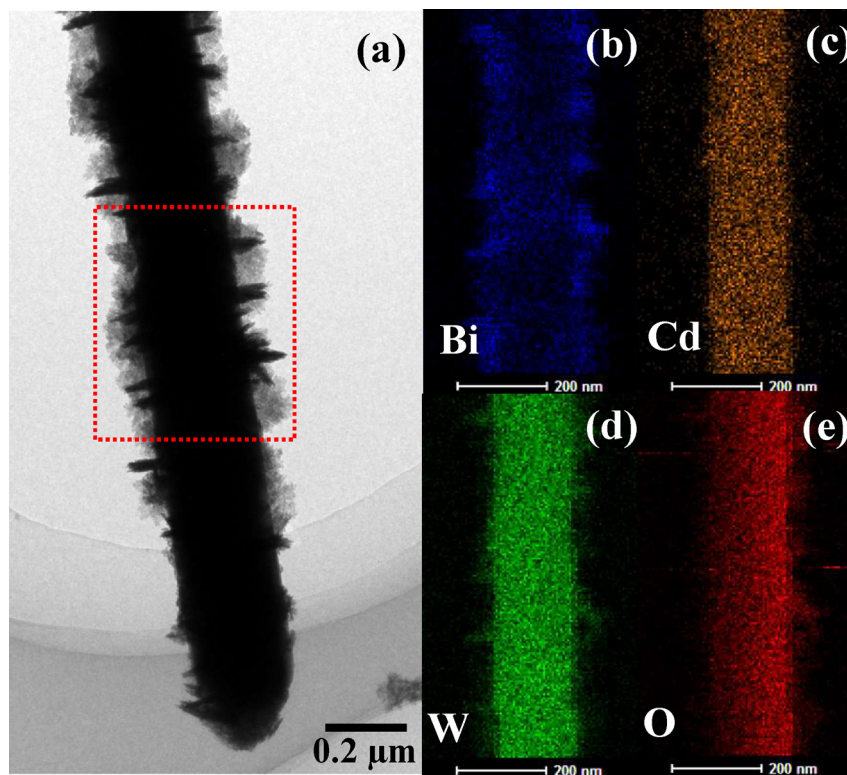


Fig. 2. (a) TEM image of BCW-4, and the corresponding elemental mappings: (b) Bi, (c) Cd, (d) W, and (e) O.

of the enhanced specific surface area and enriched active sites for light absorption and photocatalytic reaction, respectively. To obtain information about the Bi₂WO₆/CdWO₄ structure, the sample was characterized by transmission electron microscopy (TEM). As illustrated in Fig. 2a, the Bi₂WO₆ nanoplates grow vertically on the surface of the CdWO₄ rod, in consistent with the SEM results; the Bi₂WO₆ nanoplates show an average length of about 100 nm and a thickness of less than 20 nm. The element mapping data suggest uniform distribution of Bi, Cd, O and W elements throughout the Bi₂WO₆/CdWO₄ heterostructure (Fig. 2b–e). The Cd element distributes on the entire rod whereas the Bi element on the Bi₂WO₆ branches.

The formation mechanism of hierarchical Bi₂WO₆/CdWO₄ involves the presence of WO₄²⁻ at the CdWO₄ interface due to electrostatic interaction. From Fig. S1 (see in supporting information, SI†), one can see that the morphology of the as-prepared composites are quite different. The growth of Bi₂WO₆ on the surface of CdWO₄ is closely related to the concentration of Bi³⁺ in the suspension. With the addition of Bi³⁺, tiny crystalline nuclei made of orthorhombic Bi₂WO₆ grow to form irregular particles at the expense of smaller particles, a result of energy difference in solubility according to the Gibbs-Thomson law [22] (Fig. S1a, SI†). During the solvothermal process, there is the formation of oxygen defects at the Bi₂WO₆/CdWO₄ interfaces. The oxygen defects can generate quasi-continuous energy levels that induce ohmic contact and lower the interfacial electric resistance, consequently benefiting the growth of Bi₂WO₆ on the CdWO₄ microrods [23]. With the increase of Bi₂WO₆/CdWO₄ molar ratio, Bi₂WO₆ changes from nanoparticles to nanoplates (Fig. S1b, SI†). There is the formation of laminar structure that develops into nanoplates as a result of anisotropic growth along the (001) plane parallel to the intrinsic layered structure. Further increase of Bi₂WO₆ amount would result in the surface of CdWO₄ rods being covered with Bi₂WO₆ nanoplates (Fig. S1c, SI†), and finally with further increase of Bi₂WO₆ the plates aggregate (Fig. S1d, SI†). Finally, the Bi₂WO₆ nanoplates become granular (Fig. S1e, SI†), plausibly due to the increase of interfacial energy for Bi₂WO₆ formation, and Bi₂WO₆ readily aggregates to particles on the CdWO₄

microrods [19]. Based on these characterization results and experimental details, a possible mechanism for the formation of the hierarchical heterostructure is proposed and illustrated in Fig. S2 (SI†).

The XRD patterns of samples shown in Fig. S3 (SI†) demonstrate that the peaks of the BCW samples match well with those of standard CdWO₄ (JCPDS NO. 14–0676) and Bi₂WO₆ (JCPDS NO. 26–1044) [22,24] and no detection of impurities, implying successful fabrication of the target materials. In addition, the results of FTIR investigation as well as ICP-OES analysis (Fig. S4 and Table S1, SI†) provide further evidence for the formation of Bi₂WO₆/CdWO₄ and the composition of the composite samples is quite in agreement with the theoretical value.

X-ray photoelectron spectroscopy (XPS) was applied to investigate the surface composition and chemical states of elements. The survey spectrum shows the presence of Bi, O, Cd, and W (Fig. 3a). The peaks with binding energy of 159.2 and 164.8 eV in the high-resolution Bi 4f spectrum are attributed to Bi 4f_{7/2} and Bi 4f_{5/2} signals, respectively (Fig. 3b), demonstrating that the main chemical state of Bi is +3 [25]. The two peaks at about 405.2 and 411.9 eV in Fig. 3c can be ascribed to the Cd 3d_{5/2} and Cd 3d_{3/2} signals of Cd²⁺ in CdWO₄. The binding energy of the Cd 3d peaks of Bi₂WO₆/CdWO₄ exhibit an obvious shift as compared to that reported by Fujita et al [26]. These results can be explained by the intense interface interaction between Cd and Bi₂WO₆ [27]. The W 4f XPS spectrum is illustrated in Fig. 3d, and peaks at 35.5 and 37.6 eV are assignable to W 4f_{7/2} and W 4f_{5/2} signals, which can be used as fingerprint to identify the presence of W⁶⁺, while the peaks centered at 34.6 and 36.6 eV detected after deconvolution are related to the W 4f_{7/2} and W 4f_{5/2} signals of W⁵⁺ [28]. The O 1 s spectrum shown in Fig. 3e with peaks located at 530.2 and 531.1 eV are ascribable to O²⁻ ions and oxygen defects of sample, respectively [29]. CdWO₄ is composed of edge-sharing octahedral CdO₆ and WO₆ in the form of alternate zigzag chains [29]. On the CdWO₄ surface, the presence of Bi³⁺ results in the generation of oxygen defects, causing distortion of octahedral WO₆. The XPS results further confirm the coexistence of Bi₂WO₆ and CdWO₄ in the BCW-4 sample, which is consistent with the results of EDS analysis (Fig. 3f). The oxygen defects at the Bi₂WO₆/

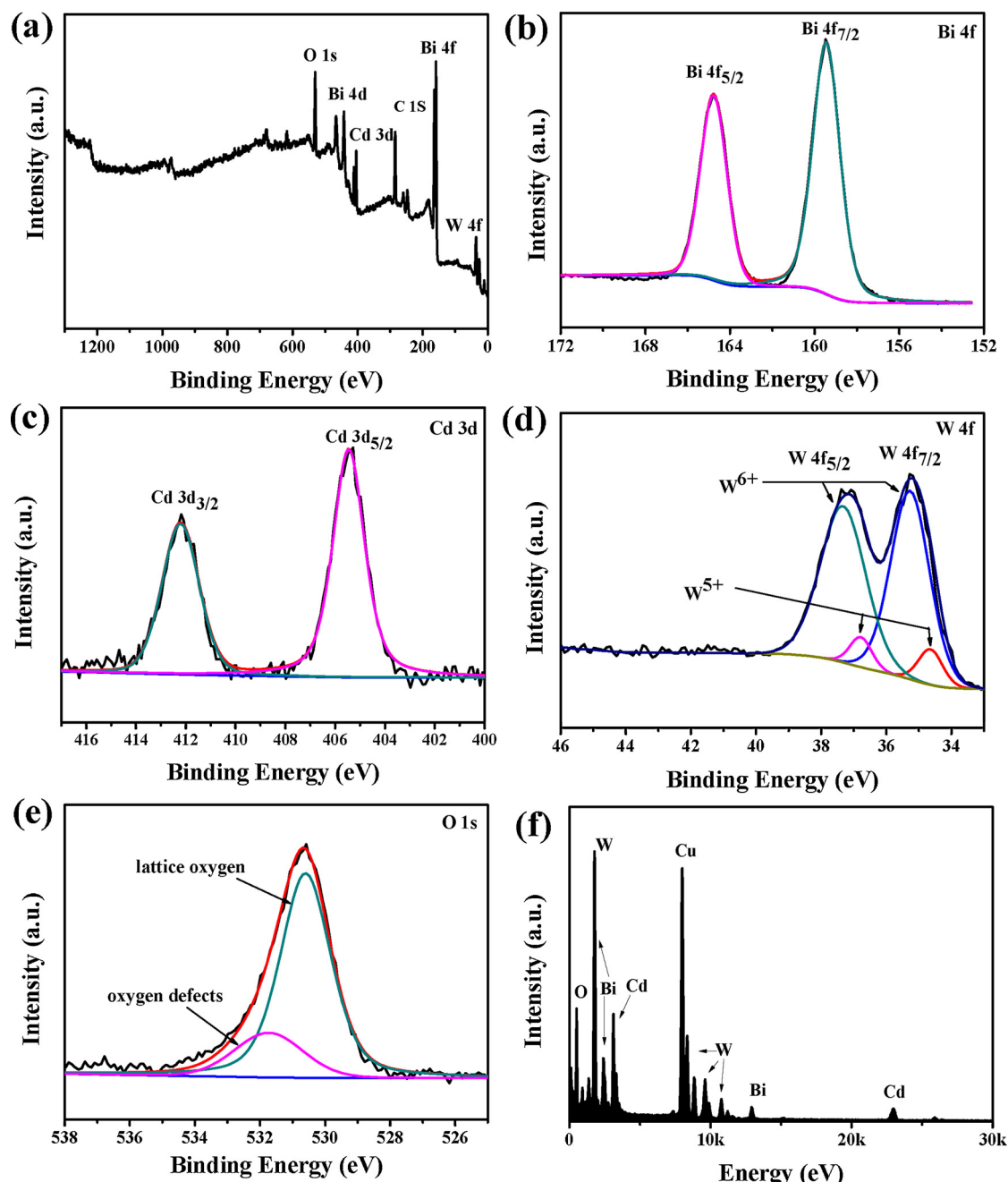


Fig. 3. XPS (a) survey, (b) Bi 4f, (c) Cd 3d, (d) W 4f, and (e) O 1s spectra and (f) EDS spectrum of BCW-4.

CdWO_4 interface can form quasi-continuous energy levels, which induce the formation of ohmic contact and lower the interfacial electric resistance [30]. The oxygen vacancy is a hole-type defect which tends to attract electrons under O-rich conditions [29]. It is hence envisaged that there is promotion of the separation of photogenerated charge carriers inside BCW-4.

UV-vis absorption spectra of Bi_2WO_6 , CdWO_4 , and the BCW samples are depicted in Fig. S5a (SI†), the BCW samples exhibit absorption similar to that of Bi_2WO_6 in the visible light region. According to the “ $(ahv)^2$ versus photon energy” plots, the bandgap of Bi_2WO_6 and BCW is 3.0 and 2.85 eV, respectively (Fig. S5b, SI†), in agreement with the reported data [23,31]. Photoelectrochemical measurements were also performed in order to further illustrate the ability of photo-induced charge separation. The photocurrent density of BCW-4 electrode is about 2.1 fold higher than that of pure Bi_2WO_6 electrode (Fig. 4a). Additionally, from the EIS Nyquist plot of the photoluminescence (PL)

spectra shown in Fig. 4b, it can be seen that the emission intensity of the samples decreases in the following order: BCW-4 < Bi_2WO_6 < CdWO_4 , indicating that charge recombination can be better suppressed after the loading of Bi_2WO_6 on CdWO_4 . The results suggest that the BCW samples have a band gap low enough for visible-light-induced electronic transition, and consequently results in photocatalytic activity under visible light irradiation.

To demonstrate the photocatalytic activity of the three dimensional (3D) hierarchical heterostructure, we used the selective hydroxylation of benzene under visible-light ($\lambda \geq 400$ nm) irradiation in the presence of dioxygen as a model reaction (Table 1). The experiment started with a mixture of acetonitrile (CH_3CN) and H_2O being stirred under aerobic condition in the dark for 30 min before being exposed to visible light. In the cases of having the reaction conducted (i) without a photocatalyst and (ii) with no irradiation, there is no generation of products. The results confirm that the reaction is photocatalytic. Among the

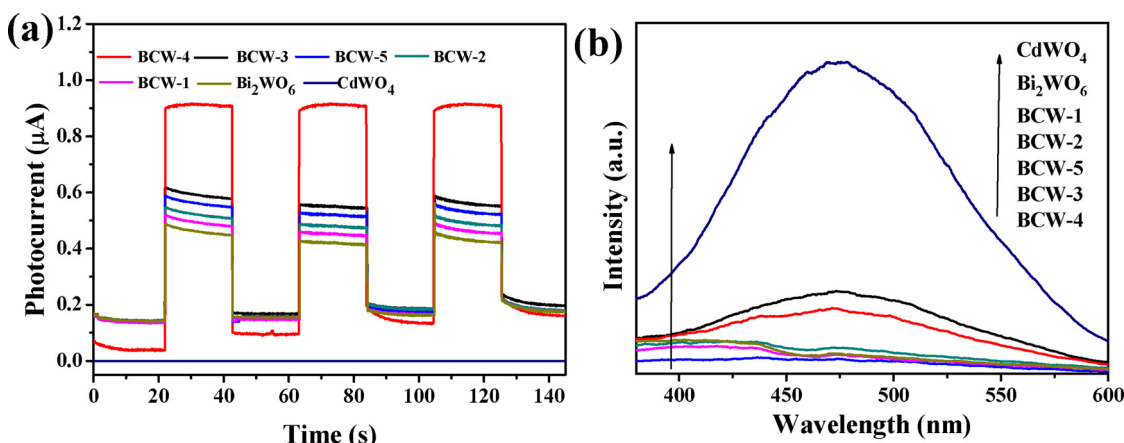


Fig. 4. (a) Photocurrent response and (b) PL spectra of Bi₂WO₆, CdWO₄ and BCW-4 ($\lambda_{\text{Ex}} = 290 \text{ nm}$).

Table 1
Selective oxidation of benzene to phenol under different reaction conditions.^a

Entry	Catalyst	Conversion (%)	Formation Rate ($\mu\text{mol g}^{-1} \text{h}^{-1}$)	Selectivity (%)
1	CdWO ₄	— ^b	—	—
2	Bi ₂ WO ₆	1.2	40.0	> 99
3 ^c	—	—	—	—
4 ^d	BCW-4	—	—	—
5 ^e	BCW-4	2.3	76.7	> 99
6	BCW-1	0.7	23.3	> 99
7	BCW-2	2.5	83.3	> 99
8	BCW-3	4.2	140.0	> 99
9	BCW-4	5.8	193.3	> 99
10	BCW-5	3.8	126.7	> 99

^a Reaction conditions: benzene (0.5 mmol), photocatalyst (50 mg), acetonitrile (3 mL), H₂O (100 μL), O₂ (3 mL min⁻¹), light irradiation ($\lambda \geq 400 \text{ nm}$), 3 h.

^b No or negligible products were detected.

^c Without photocatalyst.

^d No irradiation.

^e No O₂.

photocatalysts, BCW-4 is the most effective for the photocatalytic hydroxylation of benzene to phenol. After 3 h of irradiation the conversion of benzene is 5.8%, and selectivity to phenol is above 99%. No products of over oxidation such as diphenol or quinone derivatives are detected. It is clear that the loading of Bi₂WO₆ on CdWO₄ results in the enhancement of photocatalytic activity. It is deduced that the superior performance of BCW-4 could be attributed to the enhancement of catalyst surface area (25.7 m² g⁻¹) (Table S2, SI†) and high ability for separation of photogenerated charge carriers, both are intrinsic properties of hierarchical materials.

As depicted in Fig. 5a, an experiment of benzene hydroxylation over BCW-4 for 4 h displays a benzene conversion of 7.3%. With such performance, the BCW-4 catalyst can be considered as promising for the selective hydroxylation of benzene for phenol production. In all instances of using BCW-4 as photocatalyst there is no detection of carbon oxides, indicating the absence of over oxidation. We also studied the stability of BCW-4 in ten successive cycles of reaction (Fig. 5b), and found almost no loss of activity in ten times of reuse. The results suggest high recyclability of the as-prepared composite photocatalyst. Samples before and after ten cycles were studied by SEM, and the integrity of structure further confirms the stability of BCW-4 (Fig. S6, SI†). What is more, the BCW-4 catalysts showed high activity towards the hydroxylation of some derivative of benzene (Table S3, SI†). Endowed with high activity and stability, BCW-4 is a good catalyst, showing potential industrial application for the production of phenol under mild conditions.

For mechanistic investigation, a series of additives was employed to study the active species in the reaction process. When 1 mmol of TEMPO was added (tetra-methylpiperidine N-oxide, a radical scavenger), there was almost complete quenching of benzene conversion. We then proceeded to identify the essential radicals using specific scavengers. Shown in Fig. 6 is the benzene conversion over BCW-4 with or without a quencher. In the investigation, ammonium oxalate (AO) was used as hole (h⁺) scavenger, potassium persulphate (K₂S₂O₈) as electron (e⁻) scavenger, and tert-butanol (TBA) was used to capture hydroxyl radical (·OH) [32–34]. It is clear that electrons, holes as well as hydroxyl radicals have a role to play in this reaction. Comparing the changes of benzene conversion after the addition of different scavengers, one can see that the importance of these three kinds of species follows a trend of “·OH > h⁺ > e⁻”. In this reaction, ·OH was produced following two pathways, one on the conduction band of Bi₂WO₆ by steps illustrated in Eqs. 1–4 (SI†) [35,36], and the other of direct ·OH production from the valence band (see Eq. 5, SI†) [37–39]. The production of ·OH from the oxidation water by holes was confirmed (entry 5, Table 1) because there is phenol generated even without O₂. It is worth pointing out that after the quenching of ·OH, there is still generation of phenol (the conversion of benzene is about 0.5%), indicating the existence of a minor path for direct benzene oxidation induced by h⁺ (see Eq. 6, SI†) [40]. It is noted that despite the production of ·OH on the conduction band is a 3-electron process while that on the valence band is an one-hole process, the conversion of benzene by holes (3.7%) is not 3 times that of by electrons (2.5%). This phenomenon may be ascribed to the difference in life and transfer efficiency of electrons and holes.

Based on the results of the photocatalytic reactions conducted over different catalysts and under various conditions, a possible mechanism for selective benzene oxidation is proposed (Scheme 1). Under visible-light irradiation, the hierarchical heterostructure of Bi₂WO₆/CdWO₄ allows multiple reflections of visible light within the interior cavity for enhanced Bi₂WO₆ excitation. In the major process, the photogenerated electrons on the CB of Bi₂WO₆ move to oxygen vacancies and capture the oxygen molecules, and the as-resulted O₂^{·-} reacts with H⁺ from surface water to form H₂O₂ and subsequently hydroxyl radicals [40,41]. Furthermore, the photoinduced holes efficiently migrate to the CB of CdWO₄, and react with surface OH⁻ to form hydroxyl radicals [42]. The as-resulted hydroxyl radicals react with benzene to generate hydroxylated benzene in a form of radical. Upon further attached by a hydroxyl radical, the hydroxylated benzene is converted to phenol with H₂O as sole byproduct [43]. Another minor route is that the surface holes react with benzene to form the corresponding intermediate which further reacts with oxygen to give phenol [44].

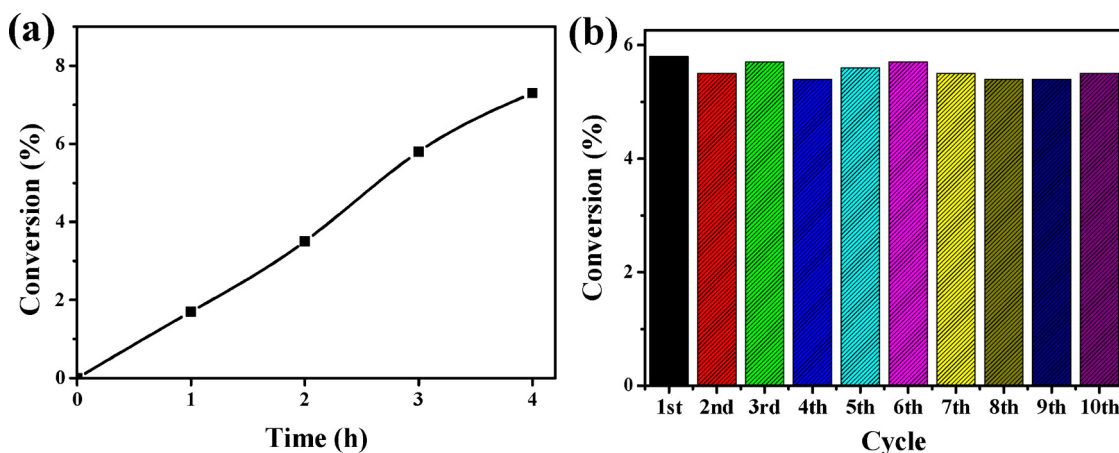


Fig. 5. (a) Conversion of benzene as a function of irradiation time, and (b) recycling property of BCW-4 in benzene hydroxylation.

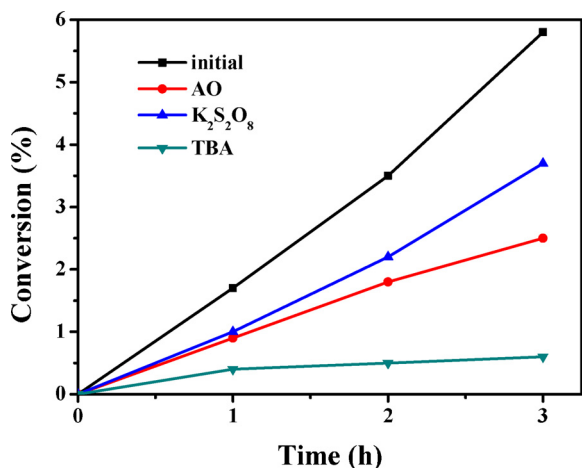
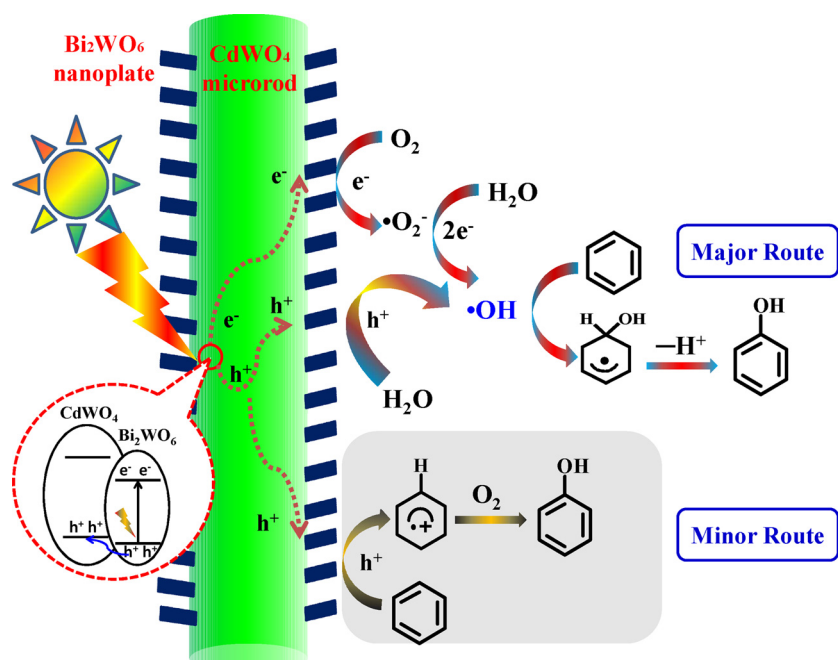


Fig. 6. Photocatalytic performance of BCW-4 (a) with or without a scavenger. Reaction conditions: benzene (0.5 mmol), photocatalyst (50 mg), acetonitrile (3 mL), H₂O (100 µL), light irradiation ($\lambda \geq 400$ nm), scavengers (1 mmol).

4. Conclusions

For the first time, a novel 3D Bi₂WO₆/CdWO₄ hierarchical heterostructure was prepared by a simple solvothermal method. In the Bi₂WO₆/CdWO₄ composite, CdWO₄ microrods are fully decorated with Bi₂WO₆ nanoplates. Based on the experimental data and characterization results, a mechanism for the formation of the hierarchical heterostructure is proposed. The Bi₂WO₆/CdWO₄ composite shows high activity as well as stability for benzene hydroxylation to phenol under visible light irradiation using O₂ as oxidant (benzene conversion up to 7.3% in 4-hour irradiation and selectivity to phenol above 99%). As a result of the unique hierarchical heterostructure, there is significant increase of visible light absorption and separation efficiency of photo-induced charge carriers, consequently the enhanced photocatalytic activity. Moreover, through the investigation of active species, we disclose the pivotal role of ·OH radicals. It is noted that the generation of ·OH radicals on the Bi₂WO₆/CdWO₄ surface can involve both photo-induced electrons and holes. Finally, a plausible mechanism for the reaction has been proposed.



Scheme 1. Plausible mechanism of photocatalytic benzene hydroxylation to phenol over the hierarchical heterostructure of Bi₂WO₆/CdWO₄.

Acknowledgements

This project was financially supported by the NSFC (Grants 21725602, 21476065, 21671062, and 21776064), the Fundamental Research Funds for the Central Universities, Hunan Provincial Natural Science Foundation (Grant 2015JJ3033), and the Hunan Provincial Science and Technology Project (2015JC3051). C. T. Au thanks the HNU for an adjunct professorship.

Appendix A. Supplementary data

Supplementary material related to this article can be found, in the online version, at doi:<https://doi.org/10.1016/j.apcatb.2018.04.028>.

References

- [1] G. Zhang, J. Yi, J. Shim, J. Lee, W. Choi, *Appl. Catal. B: Environ.* 102 (2011) 132–139.
- [2] S. Niwa, M. Eswaramoorthy, J. Nair, A. Raj, N. Itoh, H. Shoji, T. Namba, F. Mizukami, *Science* 295 (2002) 105–107.
- [3] Y. Ide, M. Torii, T. Sano, *J. Am. Chem. Soc.* 135 (2013) 11784–11786.
- [4] X.H. Li, X. Wang, M. Antonietti, *ACS Catal.* 2 (2012) 2082–2086.
- [5] K. Ohkubo, T. Kobayashi, S. Fukuzumi, *Angew. Chem. Int. Ed.* 50 (2011) 8652–8655.
- [6] K. Ohkubo, A. Fujimoto, S. Fukuzumi, *J. Am. Chem. Soc.* 135 (2013) 5368–5371.
- [7] P. Devaraji, N.K. Sathu, C.S. Gopinath, *ACS Catal.* 4 (2014) 2844–2853.
- [8] D. Wang, M. Wang, Z. Li, *ACS Catal.* 5 (2015) 6852–6857.
- [9] K.I. Shimizu, T. Kaneko, T. Fujishima, T. Kodama, H. Yoshida, Y. Kitayama, *Appl. Catal. A: Gen.* 225 (2002) 185–191.
- [10] H. Park, W. Choi, *Catal. Today* 101 (2005) 291–297.
- [11] X. Chen, J. Zhang, X. Fu, M. Antonietti, X. Wang, *J. Am. Chem. Soc.* 131 (2009) 11658–11659.
- [12] N. Zhang, R. Ciriminna, M. Pagliaro, Y.J. Xu, *Chem. Soc. Rev.* 43 (2014) 5276–5287.
- [13] Y. Zhang, N. Zhang, Z.R. Tang, Y.J. Xu, *Chem. Sci.* 4 (2013) 1820–1824.
- [14] H. Cheng, B. Huang, Y. Liu, Z. Wang, X. Qin, X. Zhang, Y. Dai, *Chem. Commun.* 48 (2012) 9729–9731.
- [15] Y. Liu, L. Chen, Q. Yuan, J. He, C.T. Au, S.F. Yin, *Chem. Commun.* 52 (2016) 1274–1277.
- [16] H. Fu, C. Pan, W. Yao, Y. Zhu, *J. Phys. Chem. B* 109 (2005) 22432–22439.
- [17] K. Wang, G. Liu, N. Hoivik, E. Johannessen, H. Jakobsen, *Chem. Soc. Rev.* 43 (2014) 1476–1500.
- [18] D. He, L. Wang, D. Xu, J. Zhai, D. Wang, T. Xie, *ACS Appl. Mater. Inter.* 3 (2011) 3167–3171.
- [19] M. Shang, W. Wang, L. Zhang, S. Sun, L. Wang, L. Zhou, *J. Phys. Chem. C* 113 (2009) 14727–14731.
- [20] M.H. Sun, S.Z. Huang, L.H. Chen, Y. Li, X.Y. Yang, Z.Y. Yuan, B.L. Su, *Chem. Soc. Rev.* 45 (2016) 3479–3563.
- [21] R.P. Jia, G.X. Zhang, Q.S. Wu, Y.P. Ding, *Appl. Surf. Sci.* 253 (2006) 2038–2042.
- [22] C. Zhang, Y. Zhu, *Chem. Mater.* 17 (2005) 3537–3545.
- [23] X. Jia, M. Tahir, L. Pan, Z.F. Huang, X. Zhang, L. Wang, J.J. Zou, *Appl. Catal. B: Environ.* 198 (2016) 154–161.
- [24] W. Tong, L. Li, W. Hu, T. Yan, G. Li, *J. Phys. Chem. C* 114 (2010) 1512–1519.
- [25] L. Yue, S. Wang, G. Shan, W. Wu, L. Qiang, L. Zhu, *Appl. Catal. B: Environ.* 176–177 (2015) 11–19.
- [26] M. Fujita, M. Itoh, T. Katagiri, D. Iri, M. Kitaura, V.B. Mikhailik, *Phys. Rev. B* 77 (2008) 155118.
- [27] D. Li, J. Xue, X. Bai, *CrystEngComm* 18 (2016) 309–315.
- [28] A.P. Shpak, A.M. Korduban, M.M. Medvedskij, V.O. Kandyba, *J. Electron Spectrosc. Relat. Phenom.* 156–158 (2007) 172–175.
- [29] C. Zhang, D. Guo, W. Xu, C. Hu, Y. Chen, *J. Phys. Chem. C* 120 (2016) 12218–12225.
- [30] X. Jia, M. Tahir, L. Pan, Z.F. Huang, X. Zhang, L. Wang, J.J. Zou, *Appl. Catal. B: Environ.* 198 (2016) 154–161.
- [31] S. Sun, W. Wang, J. Xu, L. Wang, Z. Zhang, *Appl. Catal. B: Environ.* 106 (2011) 559–564.
- [32] Y.H. Zhang, N. Zhang, Z.R. Tang, Y.J. Xu, *Chem. Sci.* 3 (2012) 2812–2822.
- [33] A. Sharma, R.K. Dutta, *RSC Adv.* 5 (2015) 43815–43823.
- [34] T.D. Bui, A. Kimura, S. Ikeda, M. Matsumura, *J. Am. Chem. Soc.* 132 (2010) 8453–8458.
- [35] L. Chen, S.F. Yin, R. Huang, Y. Zhou, S.L. Luo, C.T. Au, *Catal. Commun.* 23 (2012) 54–57.
- [36] L. Chen, Q. Zhang, R. Huang, S.F. Yin, S.L. Luo, C.T. Au, *Dalton Trans.* 41 (2012) 9513–9518.
- [37] S. Wu, H. Cao, S. Yin, X. Liu, X. Zhang, *J. Phys. Chem. C* 113 (2009) 17893–17898.
- [38] L. Chen, R. Huang, Y.J. Ma, S.L. Luo, C.T. Au, S.F. Yin, *RSC Adv.* 3 (2013) 24354–24361.
- [39] L. Chen, R. Huang, M. Xiong, Q. Yuan, J. He, J. Jia, M.Y. Yao, S.L. Luo, C.T. Au, S.F. Yin, *Inorg. Chem.* 52 (2013) 11118–11125.
- [40] S. Fukuzumi, K. Ohkubo, *Chem. Sci.* 4 (2013) 561–574.
- [41] H. Li, F. Qin, Z. Yang, X. Cui, J. Wang, L. Zhang, *J. Am. Chem. Soc.* 139 (2017) 3513–3521.
- [42] Y.H. Zhang, N. Zhang, Z.R. Tang, Y.J. Xu, *ACS Nano* 6 (2012) 9777–9789.
- [43] O. Tomita, R. Abe, B. Ohtani, *Chem. Lett.* 40 (2011) 1405–1407.
- [44] O. Tomita, B. Ohtani, R. Abe, *Catal. Sci. Technol.* 4 (2014) 3850–3860.